Journal of Hazardous Materials 387 (2020) 121693

Contents lists available at ScienceDirect

Journal of Hazardous Materials

journal homepage: www.elsevier.com/locate/jhazmat

# The reduction of Fe-bearing copper slag for its use as a catalyst in carbon oxide hydrogenation to methane. A contribution to sustainable catalysis

Ismael Fuentes[a,1], Claudia Ulloa[b], Romel Jiménez[a], Ximena García[a,*]

[a] Laboratory of Carbon and Catalysis (CarboCat), Department of Chemical Engineering, Universidad de Concepción, P.O. Box 160-C, Concepción, Chile
[b] Department of Environmental Engineering, University of Concepción, P.O. Box 160-C, Concepción, Chile

## GRAPHICAL ABSTRACT

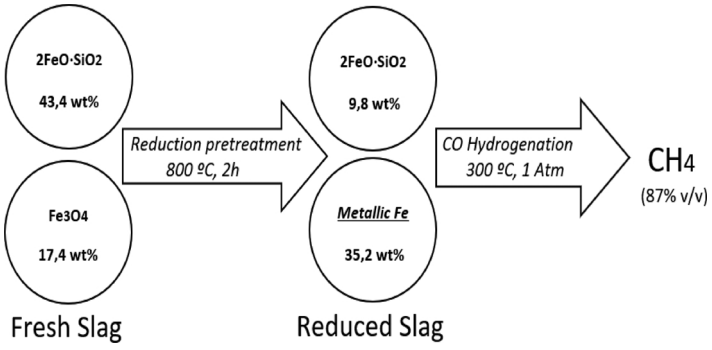


## ARTICLE INFO

Editor: G. Lyberatos

*Keywords:*
Copper slag
Catalyst
Slag reduction
CO hydrogenation
Fe-based catalyst

## ABSTRACT

Reduction of Fe-phases in a slag from the copper smelting process is studied for its use as a catalyst in methanation of carbon oxide (CO). This material contains 36.4 wt% Fe and the main Fe-phases in its fresh and reduced forms were identified and quantified. Chemical analysis and X-ray diffraction (XRD) for crystalline phase detection and determination of Fe dispersion were carried out. Reducibility of Fe-oxides was studied by thermal programmed reduction (TPR) under $H_2$ at 650 and 800 °C using 0.5 and 2 h soak time. In the fresh slag, iron was found to be in the form of $Fe_3O_4$ (17.4 wt%) and fayalite, $Fe_2SiO_4$ (43.4 wt%). The composition was experimentally determined and verified by stoichiometric balances and thermogravimetric analysis (TGA). Upon reduction at 800 °C and 2 h soak time, 87 % of the Fe-phases were reduced, leaving an activated catalyst with a 35.2 % $Fe^0$, which is the active phase for CO hydrogenation to methane. An expression was derived to determine the $Fe^0$ concentration in the reduced slag based on the composition of the fresh slag and its reduction degree. The catalytic activity of the reduced slag during CO hydrogenation was evaluated in a fixed bed differential reactor. The selectivity to methane, at 300 °C, was 87 %, thus confirming its catalytic activity for the selected reaction.

* Corresponding author at: Ximena García in Laboratory of Carbon and Catalysis (CarboCat), Department of Chemical Engineering, Universidad de Concepción, P.O. Box 160-C, Concepción, Chile.
*E-mail address:* xgarcia@udec.cl (X. García).
[1] Present Address: Department of Chemical Engineering, Faculty of Physical and Mathematical Sciences, Universidad de Chile, P.O. Box 2777, Santiago, Chile.

https://doi.org/10.1016/j.jhazmat.2019.121693
Received 16 April 2019; Received in revised form 13 November 2019; Accepted 14 November 2019
Available online 15 November 2019
0304-3894/ 

## 1. Introduction

As resources become more precious, governments have placed pressure on industries and individuals to adopt the "reduce, reuse, repair and recycle" hierarchy of resource efficiency (de la Caba et al., 2019). More recently, these concepts have been adopted into the "circular economy" philosophy, whose essential principles are to reduce resource use and environmental impacts by "closing the loop" of production (Jurgilevich et al., 2016). Accordingly, effective utilization of large scale industrial wastes has recently become a topic of considerable interest in the search for a sustainable future (Alzeer and MacKenzie, 2018).

High volume waste materials resulting from large scale industrial processes particularly afford opportunities in catalysis. To date, a few reports detailing the application of wastes to the preparation of catalysts have been published. In some of them, these materials are directly applied as catalyst or catalyst-support, while in others, they are used as precursors for the synthesis of active catalytic materials (Cheng et al., 2017; Marwaha et al., 2018).

Since the beginning of the industrial era, slags, left over when metals are extracted from ores, have been considered as wastes (Gorai and Jana, 2003). One such material is copper slag (CS), which is produced during matte smelting and converting steps of pyrometallurgical production of copper. In 2015, approximately 68.7 million tons of CS were generated by the copper industry worldwide (Sharma and Khan, 2018). China accounted for one third of world CS production, followed by Japan (9 %) and Chile (8 %) (Sharma and Khan, 2018). The increasing global demand for copper will not change this scenario with the consequent rise on the demand for landfill sites for its disposal (Shih et al., 2018).

In 1991, the U.S. Environmental Protection Agency (USEPA) classified copper slag as a hazardous waste. Five years later, in 1996, the United Nations Basel Convention on the Transboundary Movement of Hazardous Wastes and their Disposal, reclassifies it as non-hazardous material for the environment, and opened up the possibilities for its use as a replaceable resource for various industries. Several studies have been developed to investigate the degree of toxicity and determine the concentration of heavy metals in copper slag using leaching. In all of them, heavy metal concentrations were lower than the limit values recommended by USEPA (Lori et al., 2019). However, it is recognized that such slags are not always inert and that their leaching potential may be high, especially under specific applications, such as building material, or when expose to seawater. Thus, for any purpose, detailed studies of environmental impact, which must include mineralogical and geochemical characterization of the material along with leaching tests, are mandatory (Potysz et al., 2018).

Currently, this waste has a minimum industrial use (Raposeiras et al., 2018). Although some applications have been reported in the literature. For example, in concrete production, which increases its consistency, but can affect the stability. In cement manufacturing, which has resulted in few differences, both in mechanical performance and durability, compared to cement made from conventional raw materials. In geotechnical applications, due to its best compaction characteristics compared to sand and also in road pavement (Dhir et al., 2017). Recently CS has been used as a raw material in the preparation of a micro-electrolysis material useful in the degradation of organic pollutants in water (Yu et al., 2019). And as an oxygen transporter in the gasification of sewage sludge (Deng et al., 2019).

In another line, the recovery of iron and other valuable metals has been sought, by hydrometallurgical and pyrometallurgical processes. Hydrometallurgical processes, such as flotation, chemical leaching or bioleaching are effective methods for metal extraction; however, the generated wastewater is difficult to treat. Thus, pyrometallurgical processes, such as smelting and direct reduction, are still the most commonly used (Sarfo et al., 2017; Guo et al., 2018a, b).

The utilization of CS in the field of heterogeneous catalysis has attracted much attention over the last decade, since it is mainly composed of iron oxides (30 − 45 wt%), $SiO_2$ (35–40 %) $Al_2O_3$ (~10 %), CaO (~10 %), MgO (~5 %) and residual copper (0.5–2 %) (Gorai and Jana, 2003). In this context, CS has been assayed as a catalyst for mercury oxidation in coal combustion flue gas (Shih et al., 2018) and removal of phenol from aqueous effluents (Huanosta et al., 2012). In both cases, the iron oxides were identified as the active constituents of CS.

Iron is recognized as an active catalyst for different processes to produce hydrocarbons from the hydrogenation of carbon oxide (CO), particularly for Fischer-Tropsch Synthesis (FTS) and methanation reaction. Syngas (a mixture of CO:$H_2$) produced, for example, in biomass gasification processes, is used for hydrocarbons production through FTS, and has been extensively studied for more than fifty years (Cano et al., 2017). CO methanation ($CO + 3H_2 \rightarrow CH_4 + H_2O$), is a particular case of FTS. This reaction has been widely used in many industrial processes to produce substitute natural gas (SNG), for removal of trace amounts of CO from $H_2$-rich gases, and purification of the reformate gas for $NH_3$ synthesis and fuel cell application (Jin et al., 2016), among others.

Different metals are active as catalysts in the FTS, but today, Ni, Co and Fe are the only reasonable commercial catalysts for this process (Luo et al., 2009). Iron-based catalysts are preferentially used in FTS processes due to their low cost, and high activity (Li et al., 2016). Metals of group VIII in particular, catalyze the methanation reaction. Vannice (1975) compared the specific activity and product distribution of group VIII metals dispersed on $Al_2O_3$ in the synthesis of hydrocarbons from CO-$H_2$ mixtures. The specific activity follows the order of Ru > > Fe > Ni > Co > Rh > Pd > Pt. According to Mills and Steffgen Mills and Steffgen (1973), the methanation activity of various metals follows the order: Ru > Ir > Rh > Ni > Co > Os > Pt > Fe > Mo > Pd > Ag. Due to its good selectivity and moderate price, nickel is preferably used in commercial methanation plants (Rönsch et al., 2016). However, traditional Ni-based catalysts deactivate by sintering, associated with the heat evolution upon methanation, and poisoning by coke and/or sulfur deposition (Ocampo et al., 2011). Besides, leaching of toxic nickel carbonyls have generated some concerns due to their impact on the health and environment (Gao et al., 2015).

The activity of Fe catalyst on CO methanation is dependent on the type of active species. Iron-rich industrial wastes, such as CS, need to be activated before their use, in order to reduce the oxidized iron phases. In general, it has been established that the relative abundance of different iron phases (Fe-oxides, -carbides, or metallic) depends on the reduction gas ($H_2$ or CO), but also on the temperature, reduction time and the catalyst nature (Shroff et al., 1995). The role of the iron phases on CO methanation is still a controversial matter. Some authors suggest that the active compound for this reaction is the metallic Fe (Niemantsverdriet and Van Der Kraan, 1981), while others attribute catalytic activity to iron carbides (Riedel et al., 2003).

According to the previous discussion, it is very reasonable to hypothesize that a copper slag, after proper treatment (reduction of Fe-containing phases), can be used as a catalyst for the CO hydrogenation. In this work, activation (reduction) of CS is roughly studied, and its catalytic activity for CO hydrogenation is evaluated at methanation conditions. The raw material (CS), and the derived catalyst, were submitted to a series of analytical techniques for chemical and mineralogical characterization, in order to identify physicochemical characteristics, which explain its catalytic potential for CO hydrogenation.

## 2. Materials and methods

### 2.1. CS characterization

The CS sample was provided by the Chilean Copper Company CODELCO (División El Teniente). The sample was ground and sieved to

particle sizes ranging from 53 μm to 380 μm, and kept in a dry place for further use.

Characterization of CS was performed by several analytical techniques. The bulk composition of major inorganic elements was determined by using an X-ray fluorescence (XRF) spectrometer (RIGAKU, model Primus II), while minor elements (Cu, Zn, Pb, As, Co and Ni) were determined by atomic absorption spectroscopy (AAS), using a spectrometer GBC-905. Prior to AAS analysis, the sample was digested completely by nitric acid, according to the methodology indicated by Cardona (Cardona et al., 2013). In addition, scanning electron microscopy-energy dispersive X-ray spectroscopy (SEM-EDS) was used to verify Fe content. A TESCAN scanning electron microscope, model VEGA3 SBU EasyProbe was utilized.

Crystalline phases in raw, pretreated (activated under different conditions), and used (used in the CO hydrogenation reaction) CS were identified using X-ray diffraction (XRD). A RIGAKU Geigerflex diffractometer equipped with the D-Max/A system for the acquisition of diffraction patterns was used. This possesses a radiation source from anode FeK-α with a λ of 0.19373 nm and Mn filters and operates at 35 kV and 15 mA. The scanning speed was 1 °C/min with a step of 0.020° in a range between $3° < 2\theta < 90°$.

The content of magnetite was determined on a SATMAGAN magnetic balance (model 135), using pure magnetite and mixtures of magnetite–silica as calibration standards. Stoichiometric mass balances were applied to determine fayalite concentration, by considering the total contents of Fe (XRF) and $Fe_3O_4$.

### 2.2. Reducibility tests

The Fe present in the copper slag has to be reduced, ideally to metallic iron ($Fe^0$), to be active for CO hydrogenation. Therefore, the reducibility of CS samples was studied by temperature programmed reduction (TPR) on a chemisorption ChemBET TPR/TPD apparatus, equipped with a TCD, (Quantachrome Instrument Analyzer). A slag sample (≈ 180 mg) previously characterized and classified in particle sizes in the range 53 − 380 μm, is loaded in a U-shaped quartz tube (ID:10 mm) and heated under 40 mL/min of pure $H_2$ at 5 °C/min, from room temperature up to the selected temperature (650 °C and 800 °C). A porous quartz disk is used as a catalyst support. The sample is maintained at this temperature for a period of time (soak time = 0.5 or 2 h). The reducing gas is then exchanged to pure $N_2$ (40 mL/min), and the sample is kept under this atmosphere during another 20 min for surface cleaning, before cooling to room temperature.

In a second stage, the reduced sample is heated again at 5 °C/min in a flow of 30 mL/min of a gaseous mixture of 5 vol% $H_2$/Ar, up to 800–900 °C. $H_2$ consumption, due to catalyst reduction, was determined by a thermal conductivity detector (TCD). The change in conductivity of the gas passing through the sample in this second reduction step was followed and recorded as a function of temperature and reduction time. Reduction of a not previously reduced sample is also carried out for comparison. The total consumption was calculated from the area under the resulting TPR profile. A calibration assay using CuO as a reference material was also performed to quantify the $H_2$ consumption.

### 2.3. Thermogravimetric analysis

The degree of reduction achieved at different pretreatment conditions was determined by thermogravimetric analysis (TGA), in conjunction with stoichiometric mass balances. These allowed the calculation of the theoretical mass change associated with the complete reduction/oxidation of Fe-oxides present in the sample. The TGA tests were carried out in a TGA thermogravimetric apparatus Netzsch STA 409 PC series. The slag was heated up to 800 °C at 10 °C/min, and kept at this temperature for 2 h, under 40 mL/min of pure $H_2$. Some oxidation essays were also performed. In these, the slag sample was heated up to 1000 °C at 5 °C/min, in 50 mL/min of air. Both tests were repeated under a stream of $N_2$ as a baseline.

### 2.4. Catalytic activity

The catalytic activity of CS samples for the CO methanation was measured in a fixed bed quartz reactor (ID:10 mm) under differential regime. A K-thermocouple is used for temperature measurement. Flow of inlet gases (Total flow: 150 mL/min) is controlled by mass flow controllers (BROOKS 5850E). The CO hydrogenation reaction was carried out at 300 °C for an $H_2$ partial pressure of 40 kPa and CO partial pressure of 1.1 kPa, using 10 kPa Ar as the reference gas. A catalytic bed containing 60 mg of catalyst (without dilution) was used. Before reaction, the CS sample was reduced under $H_2$ (40 mL/min) at 800 °C for 2 h, conditions selected from the results of reducibility tests. The CO, methane ($CH_4$) and carbon dioxide ($CO_2$) compositions in outlet gases were quantified using a mass spectrometer OmniStar GSD 320. Experimental runs were kept until steady-state conditions were achieved. Both CO consumption and $CH_4$ production, expressed as turnover frequency (TOF), were calculated by Eqs. (1) and (2), respectively. They are valid at differential reactor-conditions (CO conversion less than 15 % and negligible volumetric changes).

$$TOF_{CO} = \frac{(y_{CO,\,in} - y_{CO,\,out}) \bullet F_t}{\gamma_{CO} \bullet \alpha \bullet m} \bullet \frac{M_{Fe}}{D \bullet \%Fe} \quad (1)$$

$$TOF_{CH4} = \frac{(y_{CH4,\,out} - y_{CH4,\,in}) \bullet F_t}{\gamma_{CO} \bullet \alpha \bullet m} \bullet \frac{M_{Fe}}{D \bullet \%Fe} \quad (2)$$

$y_{CO,in}$, $y_{CH4,in}$, $y_{CO,out}$ and $y_{CH4,out}$ correspond to molar fractions in the feed and product streams respectively. $F_t$ is the total molar gas flow, $M$ the molecular weight, $\gamma_{CO}$ the stoichiometric coefficient of CO, α the ideal gas molar volume (24.45 L/mol), $m$ the total mass of fresh slag, $\%Fe$ the total Fe content in the fresh slag and $D$ the Fe dispersion.

The Madon-Boudart criterion (Madon and Boudart, 1982) was used to rule out heat and mass transfer limitations in the catalytic bed, thus confirming that the reaction takes place in a fully kinetic regime. The Weisz-Prater criterion was also calculated to confirm the absence of intraparticle mass transport limitations.

## 3. Results and discussion

### 3.1. Characterization of slag

#### 3.1.1. Characterization of metallic elements

Table 1 presents the mass concentration of major metals (as oxides) in the fresh slag. Total iron content is 36.4 wt%, which gives to this selected slag a strong potential for its use as a CO hydrogenation catalyst. These results are within the range of concentrations found for this type of materials (Gorai and Jana, 2003). Minority metals are also presented in the fresh slag, with Cu and Zn (Table 1) showing the highest concentrations, although they are below 1 wt%.

Results from the SATMAGAN balance showed a 17.4 wt% of $Fe_3O_4$ (magnetite) in the fresh slag.

Fig. 1 presents the SEM-EDS analysis of a sample of fresh slag, in which large aggregates (more than 30 μm) are highlighted, these supports or are surrounded by floccules and smaller particles. Both groups show a heterogeneous particle size distribution.

Iron is homogeneously distributed on the solid surface and, as Fig. 1 shows, only a part of it is coincident with Si distribution. This means

**Table 1**
Concentration of metallic elements determined by XRF and AAS.

| Oxide | $Fe_2O_3$ | $SiO_2$ | $Al_2O_3$ | $CaO$ | $K_2O$ | $Na_2O$ | $MgO$ | $TiO_2$ |
|---|---|---|---|---|---|---|---|---|
| wt% | 52.0 | 34.2 | 7.0 | 3.8 | 1.4 | 1.2 | 0.76 | 0.51 |
| Metal | Zn | Cu | Pb | As | Co | Ni | | |
| wt% | 0.73 | 0.61 | 0.05 | 0.04 | 0.01 | < 0.004 | | |

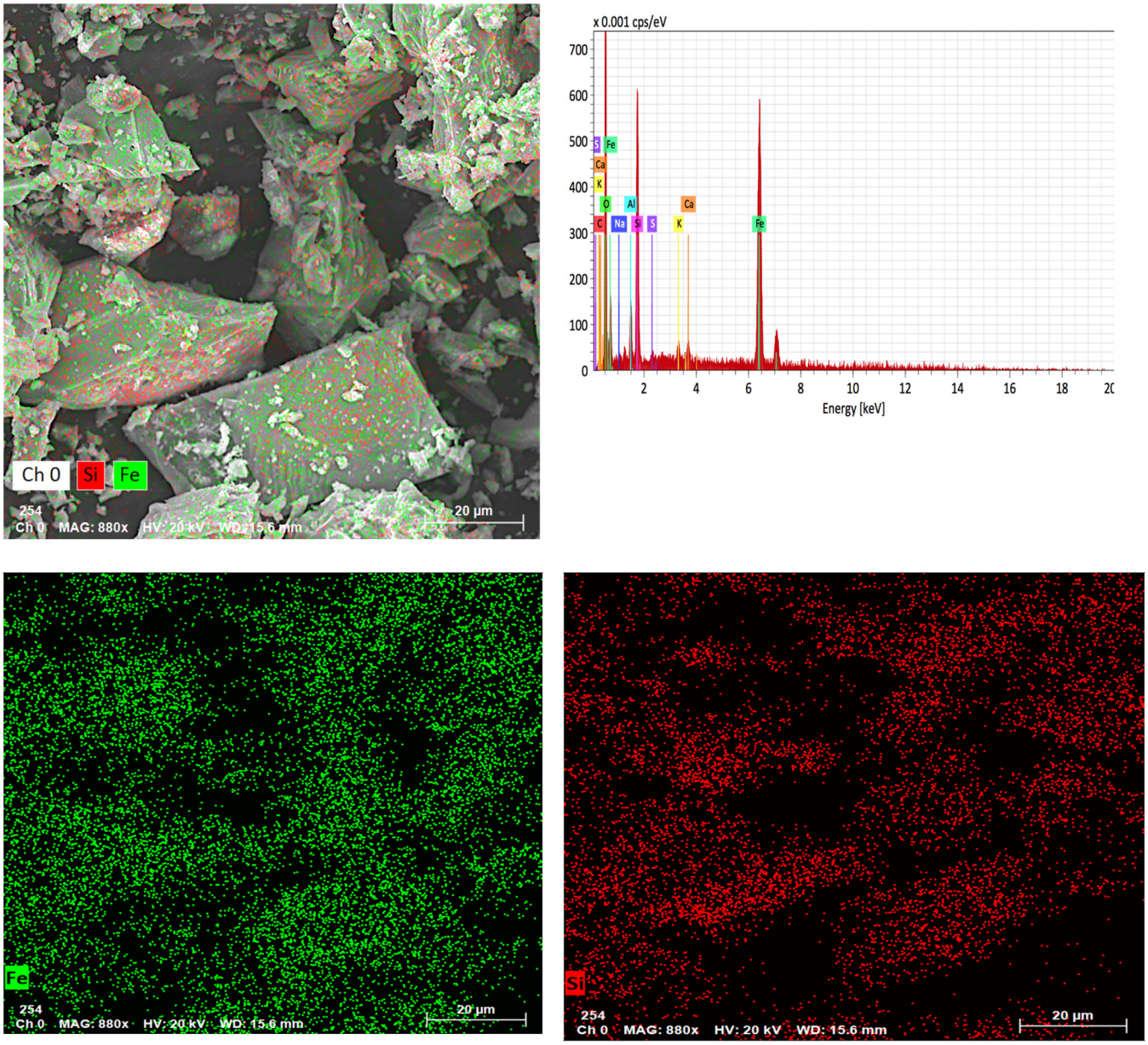


**Fig. 1.** SEM-EDS micrographs for fresh slag. Distribution of surface elements.

that only a fraction of total Fe is bounded to silicon (as fayalite). More information regarding iron phases is given below. Total iron content, determined by EDS, was 37 % wt%. Other detected elements were Si (12.0 wt%), Al (3.8 wt%), K (1.0 wt%) and Ca (0.90 wt%). These results are consistent with FRX analyses.

### 3.1.2. Reducibility

Reduction profiles obtained from the TPR assays are presented in Fig. 2. In fresh slag, $H_2$ consumption starts at 430 °C approximately. The presence of a single reduction peak indicates that under the studied conditions, simultaneous reduction of all Fe phases occurs. In fact, considering 187 mg of slag, its composition (17.4 wt% $Fe_3O_4$ and 43.4 % fayalite) and stoichiometry, $H_2$ consumptions of 564 µmol and 796 µmol are necessary for a complete reduction of $Fe_3O_4$ and FeO (in fayalite) to metallic Fe, respectively. $H_2$ consumption, calculated from the TPR diagrams was 778 µmol (up to 800 °C), a result that confirms that both phases have been reduced to metallic Fe. However, since $Fe_3O_4$ reduces more easily because it does not interact with silica (Wan et al., 2006), these results suggest that, at 800 °C, $Fe_3O_4$ was completely reduced, while only a part of FeO (26.9 %) was converted to $Fe^0$ and higher temperatures are necessary for this phase to reach complete reduction. Calculations of $H_2$ uptake from TPR analysis indicate that 57.2 % of Fe oxides have been reduced at this temperature.

The effect of pretreatment (reduction) time is observed by comparing the two curves obtained at 650 °C. The sample pretreated in $H_2$ for 2 h, reaches a higher level of reduction than the one pretreated for 0.5 h. On the other hand, the effect of pretreatment temperature in $H_2$ is observed by comparing the TPR curves of pretreated samples obtained at 650 °C and 800 °C, both with 2 h soaking time. It can be seen that an increase in reduction temperature from 650 °C up to 800 °C significantly favors the reduction process.

After a 2 h reduction at 800 °C, a low consumption of $H_2$ in the second TPR assay is observed, suggesting that such pretreatment is sufficient to reduce the Fe phases to metallic Fe. Then, these pretreatment conditions (800 °C, 2 h) are selected to activate the slag prior to its use as a catalyst during the CO hydrogenation assays.

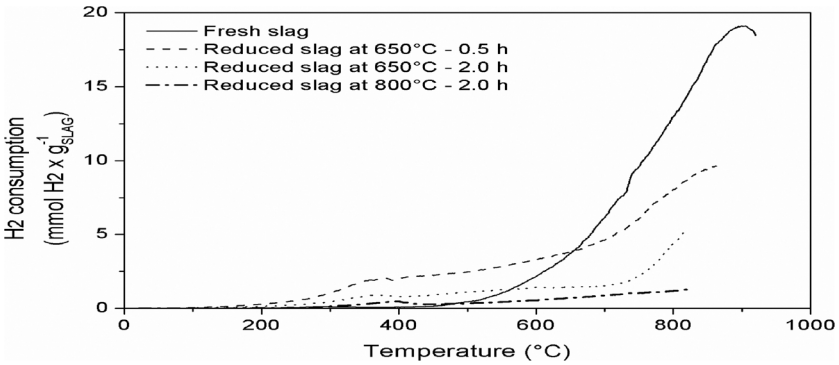


**Fig. 2.** Reduction profile of $Fe_yO_x$ in slag. Current attenuation in TCD of 16 and 150 mA.

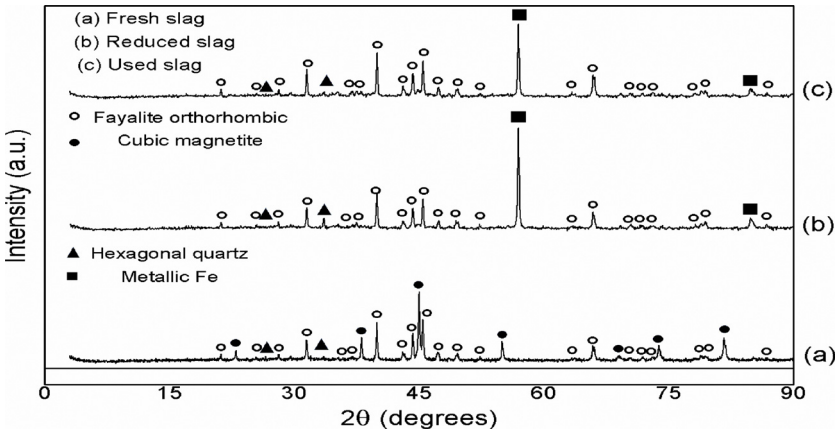


**Fig. 3.** XRD analysis for fresh, reduced and used slags.

### 3.1.3. X-ray diffraction

XRD patterns for fresh, pretreated and used slag are presented in Fig. 3. XRD analysis of fresh slag confirms the presence of fayalite ($Fe_2SiO_4$, 00 − 034 − 0178) and magnetite ($Fe_3O_4$, 00 − 019 − 0629). As mentioned, fayalite corresponds to a desirable phase in the copper smelting process that stabilizes FeO by Fe-$SiO_2$ interactions, hindering the reduction of FeO →$Fe^0$. Although this is desirable in the copper purification process, it causes an unfavorable effect for our study by displacing reduction temperatures to higher values (Wan et al., 2006). Quartz ($SiO_2$, 00 − 046 − 1045) was also detected.

Magnetite is not observed in the reduced slag, which confirms the adequacy of the selected pretreatment conditions to form metallic iron ($Fe^0$, 01 − 087 − 0721), which is considered the active phase for CO hydrogenation to methane (and in general for FTS) (Niemantsverdriet and Van Der Kraan, 1981). Furthermore, a decrease in the main peak of fayalite in this sample with respect to the fresh slag is observed. This net decrease considers both the increase in concentration due to the loss of slag during reduction, and the decrease due to the partial reduction of this phase. It was not possible to quantify the decrease in concentration from the ratio between the peak heights (in fresh and reduced slag) because, in general, no linear relationship exists between these two variables as they also depend on the micro-absorbance orientation of the particles during experimental preparation, and on mineral nature (Norrish and Taylor, 1962). On the other hand, an increase of the main peak of quartz is observed, which is attributed to the cleavage of the Fe-$SiO_2$ bond, because of the reduction of FeO from fayalite, to metallic Fe, and/or due to the loss of slag during reduction. These results, together with those of the TPR tests previously discussed, demonstrate that $Fe_3O_4$ is completely reduced, mainly to metallic Fe, while reduction of FeO content in fayalite is partial (the rest remains as a part of fayalite).

The XRD diffractogram of the used slag in the hydrogenation reaction (reaction time of 10 h), shows the same crystalline elements present in the reduced slag. There would be no formation of new crystalline phases (such as Fe carbides) as a result of the reaction. The absence of Fe carbides is attributed to the high $H_2$/CO ratio used during the reaction tests ($H_2$/CO ratio equivalent to 35), very low CO partial pressure (0.08 atm) and total pressure (1 atm). These methanation conditions differ from those present in the Fisher-Tropsch Synthesis (FTS), in which the formation of iron carbides has been observed (Rojas et al., 2006). Furthermore, it has been reported that at temperatures above 125 °C, the surface coverage by carbides and carbon deposition increases significantly with the partial pressure of CO (Ziegler and Lo, 2007), which is not the case of this study. Thus, the active phase in this work would be metallic Fe, as reported previously (Niemantsverdriet and Van Der Kraan, 1981).

On the other hand, a decrease in the main peak of metallic Fe is observed in the used sample. This could be explained by a re-oxidation of this element due to the presence of oxygenated products, such as $H_2O$ and $CO_2$ (Nakhaei et al., 2010). The high $H_2$/CO ratio and the absence of carbon detection by XRD rule out the deposition of amorphous carbon in the used slag (Mills and Steffgen, 1973).

Scherrer equation (Langford and Wilson, 1978) was used to determine the crystallite size of Fe phases (Table 2). The average crystal size of $Fe^0$ for reduced slag is used to estimate the amount of Fe at the catalytic surface (dispersion), which was calculated as 2.2 %. This value

**Table 2**
Average crystal size of iron phases in fresh, reduced and used slags, as determined by the Scherrer equation.

| $d_p$ phase (nm) | Fresh slag | Reduced slag | Used slag |
|---|---|---|---|
| $Fe_3O_4$ | 52.7 | Not detected | Not detected |
| $Fe_2SiO_4$ | 58.0 | 58.3 | 54.5 |
| $Fe^0$ | Not detected | 55.3 | 52.6 |

**Table 3**
Relationships for the main phases in the fresh (f) and reduced (r) slag.

| | |
|---|---|
| Fresh slag: | $m_{Fe^0,f}$: *Not detected (XRD)* |
| | $m_{F3O4,f}$: *Measured in SATMAGAN* |
| | $m_{Fayalite,f} = \left(\frac{m_{total\ Fe,f}}{M_{Fe}} - \frac{3m_{Fe3O4,f}}{M_{Fe3O4}}\right)\frac{M_{Fayalite}}{2}$ |
| | $m_{Quartz,f} = m_{total\ SiO2,f} - m_{Fayalite,f}\frac{M_{SiO2}}{M_{Fayalite}}$ |
| | $m_{Others,f} = m_{Freh\ slag} - m_{Fe3O4,f} - m_{Fayalite,f} - m_{Quartz,f}$ |
| | $m_{Total,f} = m_{Fresh\ slag}$ |
| Reduced slag: | $m_{Fe^0,r} = \psi \cdot m_{total\ Fe,f}$ |
| | $m_{F3O4,r}$: *Not detected (XRD)* |
| | $m_{Fayalite,r} = \left(\frac{m_{total\ Fe,f}}{M_{Fe}} - \frac{m_{Fe^0,r}}{M_{Fe}}\right)\frac{M_{Fayalite}}{2}$ |
| | $m_{Quartz,r} = m_{total\ SiO2,f} - m_{Fayalite,r}\frac{M_{SiO2}}{M_{Fayalite}}$ |
| | $m_{Others,r} = m_{Reduced\ slag} - m_{Fe^0,r} - m_{Fayalite,r} - m_{Quartz,r}$ |
| | $m_{Total,r} = m_{Reduced\ slag}$ |

is used in the calculations of the $CH_4$ formation ($TOF_{CH4}$) and CO consumption ($TOF_{CO}$) turnover rates. The diffraction angles of the major peak for each iron phase used for these calculations are 44.96° ($Fe_3O_4$); 45.44° ($Fe_2SiO_4$) and 56.92° ($Fe^0$). The similarity among the obtained values (see Table 2) shows that the pretreatment and reaction conditions have no significant effect on the average particle size of Fe phases in the slag.

### 3.1.4. Quantification of Fe phases

According to the XRF analysis (Table 1), the fresh slag contains 36.4 wt% total Fe and 34.2 wt% total silica. In addition, XRD showed that in fresh slag, Fe-containing phases correspond to fayalite ($Fe_2SiO_4$) and magnetite ($Fe_3O_4$). From this information and using stoichiometric balances, relationships for the phases in the fresh slag were derived. These are shown in Table 3.

Quartz is determined from the difference between total $SiO_2$ and $SiO_2$ content in fayalite.

According to the Satmagan measurements, the fresh slag contains 17.4 wt% de $Fe_3O_4$. Therefore, the phase composition of the fresh slag was determined from the equations of Table 3. The values, based on 100 g of fresh slag, are presented in Table 4.

To validate the concentrations of magnetite and fayalite in the fresh slag, calculations from thermogravimetric data were applied to a completely oxidized slag. Fig. 4 shows thermograms of fresh slag submitted to oxidation in air. The temperature was raised up to 1000 °C, since at this temperature, complete oxidation of the Fe oxides to hematite ($Fe_2O_3$) is achieved (Gorai and Jana, 2003). The net increase in mass, due to oxidation of iron oxides is 4.27 % (Fig. 4). This increase is mainly due to the oxidation $Fe_3O_4 \rightarrow Fe_2O_3$ for magnetite, and $FeO \rightarrow Fe_2O_3$ for FeO contained in fayalite. This mass increase is caused by the higher content of oxygen in the oxidized slag.

The theoretical weight gain due to complete oxidation of the Fe phases of slag may be determined from eq. (3):

$$\frac{\Delta m_o}{m} = \%Fe_3O_4\left(\frac{3}{2}\frac{M_{Fe2O3}}{M_{Fe3O4}} - 1\right) + \%Fayalite\frac{2M_{FeO}}{M_{Fayalite}}\left(\frac{M_{Fe2O3}}{2M_{FeO}} - 1\right) \quad (3)$$

By replacing the $Fe_3O_4$ and fayalite contents of 17.4 % and 43.4 %, respectively, in eq. 3, a weight gain of 4.07 % is obtained, which practically corresponds to the experimental TGA value (4.27 %). This result verify the above mentioned concentrations of magnetite and fayalite in the fresh slag.

**Table 4**
Mass distribution of main phases in fresh and reduced slag (wt%).

| Sample type | $Fe_3O_4$ | Fayalite | $Fe^0$ | Quartz | Others |
|---|---|---|---|---|---|
| *Fresh slag* | 17.4 | 43.4 | – | 21.4 | 17.8 |
| *Reduced slag* | – | 9.8 | 35.2 | 35.2 | 19.8 |

Fig. 5 shows a weight loss of slag when exposed to reduction (10 °C/min up to 800 °C and 2 h soak time). This is mainly due to the loss of $H_2O$ molecules that occurs during reduction of Fe oxides, as this goes from $Fe_3O_4$ to $Fe^0$ and from FeO (in fayalite) to $Fe^0$. The reduction process begins at approximately 420 °C, which agrees with TPR results (Fig. 2). As Fig. 5 shows, the net weight loss of the slag sample corresponds to 10.1 %, under the pretreatment conditions applied in this work.

If this weight loss is attributed only to complete reduction of the slag Fe phases, Eq. (4) is valid:

$$\frac{\Delta m_r}{m} = \%Fe_3O_4\left(1 - \frac{3M_{Fe}}{M_{Fe3O4}}\right) + \%Fayalite\frac{2M_{FeO}}{M_{Fayalite}}\left(1 - \frac{M_{Fe}}{M_{FeO}}\right) \quad (4)$$

Replacing a 17.4 wt% for $Fe_3O_4$ and 43.4 wt% for fayalite in Eq. (4) a theoretical weight loss of 11.6 % is calculated. The difference with respect to the experimental value (10.1 %) is attributed to the presence of Fe that has not been reduced, i.e., the FeO contained in fayalite. This is in accordance with the XRD pattern of the reduced sample in which, besides metallic Fe, the presence of fayalite was still observed. The reduction degree defined by Eq. (5) is shown in Fig. 6.

$$\psi = \frac{\%\ Experimental\ weight\ loss}{\%\ Theoretical\ weight\ loss\ (eq.\ 4)} \quad (5)$$

The reduction degree reaches a maximum value of 0.87 (87.0 %). From this, 62.7 % is achieved during the dynamic stage (heating) while the remaining 24.3 %, during the isothermal stage at 800 °C. With respect to the soak time, 18.8 % of reduction is reached in the first hour of isothermal reduction while the remaining 5.5 % during the second hour.

The degree of reduction in Fe containing samples can be determined by other methods. One of these is FTIR spectroscopy. The main advantages of this technique are its speed, reliability and no need for an inert atmosphere (Dilmac et al., 2012). Other authors have used hydrogen chemisorption for Ni catalysts (Li et al., 2000; Bartholomew and Farrauto, 1976) and magnetization measurements at saturation (Derouane et al., 1978). However, despite of this, the thermogravimetric method remains the most widely used (Lee et al., 2016; Piotrowski et al., 2005).

By applying stoichiometric mass balances, the mass of metallic Fe in a reduced slag, in terms of the reduction degree ($\psi$) ($0 \leq \psi \leq 1$) and the weights of the iron phases in the fresh slag can be calculated using Eq. (6). This expression also shows that the reduction degree depends, not only on the mass content of metallic Fe, as reported by Lee et al. (2016), but also on the mass contents of the Fe phases that are still present.

$$m_{Fe^0,r} = \psi m_{Total\ Fe} - \frac{M_{Fe}}{M_{Fe_3O_4}}(m_{Fe_3O_4,f} - \psi m_{Fe_3O_4,f} - m_{Fe_3O_4,r}) \quad (6)$$

In our case, no magnetite was present in the reduced slag ($m_{Fe_3O_4,r} = 0$). Thus Eq. (6) reduces to:

$$\boldsymbol{m_{Fe^0,r} = \psi m_{Total\ Fe} - \frac{M_{Fe}}{M_{Fe_3O_4}} m_{Fe_3O_4,f}(1 - \psi)} \quad (7)$$

And the mass concentration of metallic Fe in the reduced slag would be:

$$\boldsymbol{\%Fe_r^0 = 100\psi - \frac{100M_{Fe}}{M_{Fe_3O_4}}\frac{m_{Fe_3O_4,f}}{m_{Total\ Fe}}(1 - \psi)} \quad (8)$$

At higher reduction degrees (over 0.6), an approximately linear correlation between $Fe^0$ concentration and the reduction degree may be assumed (Eq. (9)). Table 3 shows the relationships for the phases in the reduced slag derived from Eq. (9) and stoichiometric balances.

$$\boldsymbol{\%Fe_r^0 \approx 100\psi} \quad (9)$$

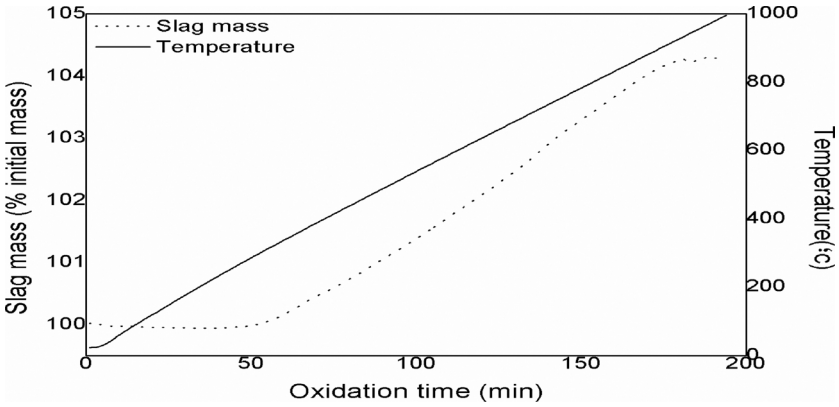


**Fig. 4.** Thermogravimetric test for oxidation pretreatment.

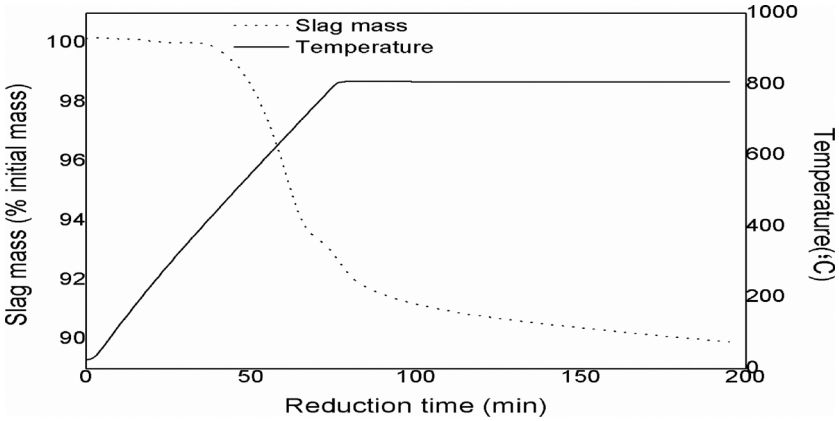


**Fig. 5.** Thermogravimetric test for reduction pretreatment.

The degree of reduction depends on several conditions; such as temperature, $H_2$ partial pressure, total pressure and reducing gas flow (Oh and Noh, 2017; Wang et al., 2019). Thus, the content of metallic Fe will also depend on these factors.

The mass of metallic Fe ($Fe^0$) in 100 g fresh slag turned out to be 31.6 g. From this result, the concentrations of the main Fe phases and other phases in the reduced slag are obtained and shown in Table 4. As observed, metallic iron is the main component (in a mass basis) in the reduced slag. This characteristic converts this pretreated copper slag in a potentially active catalyst for CO hydrogenation to methane. On the other hand, by comparing the fayalite and quartz contents in the fresh and reduced slag, a decrease of 77.4 % and an increase of 64.5 % respectively, are observed. This result agrees well with the XRD patterns of Fig. 3, which show a relative decrease of the main peak of fayalite and an increase of quartz, upon reduction, although a part of the increase may be a consequence of the weight loss of 10.1 % experienced by the sample during reduction under the applied conditions.

### 3.2. Catalytic tests

Fig. 7 demonstrates the catalytic activity of the reduced slag during CO methanation. This confirms that the selected reduction conditions were suitable for the formation of an active Fe based catalyst for the CO methanation reaction, with metallic Fe as the active component. These results also confirm that Fe oxides (in fresh slag) are inactive for CO methanation, as reported by other authors (Rojas et al., 2006). Ziegler and Lo (2007) and Govender et al. (2008), established that, $CH_4$ formation is likely to occur by stepwise hydrogenation of carbon adsorbed

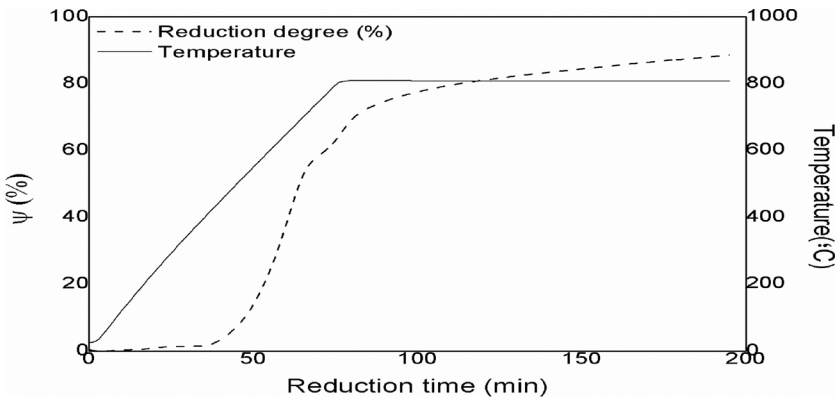


**Fig. 6.** Reduction profile during pretreatment.

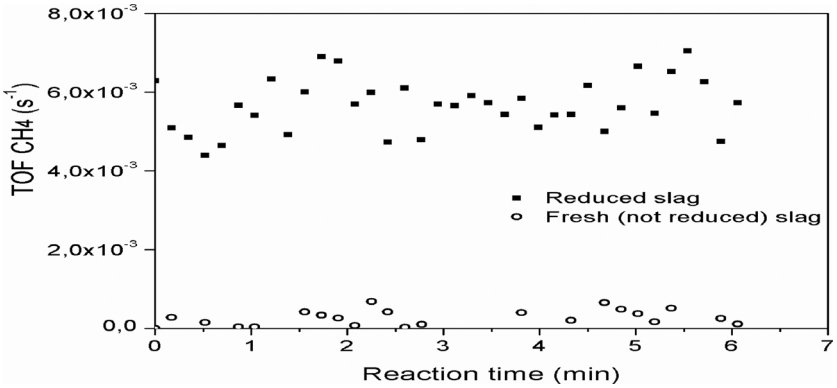


**Fig. 7.** Effect of slag activation on $CH_4$ formation rate during CO methanation. T = 300 °C, $P_{H2}$ = 40 kPa, $P_{CO}$ = 1.1 kPa.

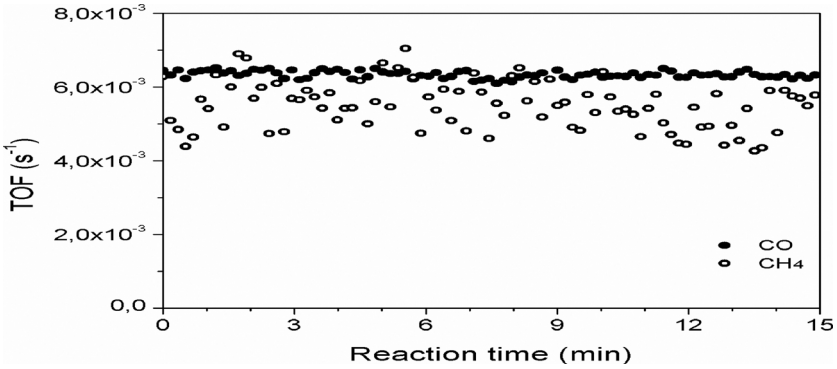


**Fig. 8.** TOF in CO hydrogenation at 300 °C, 40 kPa $H_2$ and 1.1 kPa CO, at steady state.

on the catalytic surface after CO dissociation.

Fig. 8 shows the TOF values for CO consumption and $CH_4$ formation. Its similarity demonstrates that methane is the main product of the hydrogenation of CO at the selected operating conditions (300 °C, 1 atm, 40 kPa of $H_2$ and 1.1 kPa of CO). In fact, the average selectivity to $CH_4$ was 87 % v/v, which is slightly higher than that reported by Vannice (1977) (60–75 %), at 250 °C and 1 atm for a 5 % $Fe/SiO_2$ catalyst.

## 4. Conclusions

A slag originated from a copper melting process, with a 36.4 wt% Fe, mainly in the form of magnetite ($Fe_3O_4$, 17.4 wt%) and fayalite ($Fe_2SiO_4$, 43.4 wt%), was reduced and used as a catalyst for CO methanation. The degree of reduction, after 2 h treatment under $H_2$ at 800 °C, was 87 %. The reduced slag was composed of 35.2 wt% of $Fe^0$ and 9.8 wt% of fayalite. Experimental evidences (XRD, SATMAGAN, TGA) and mass balances were consistent and demonstrated that during pretreatment (reduction process) the Fe phases were mostly reduced to $Fe^0$, which corresponds to the active phase for CO hydrogenation to methane as demonstrated by the CO methanation assays. The selectivity to methane was 87 % at the assayed conditions. The inactivity of Fe oxides was also confirmed.

An expression was derived to determine the content of metallic Fe in the reduced slag, from the reduction degree and the composition of Fe phases in the fresh slag.

The proposed methodology constitutes an important tool to characterize heterogeneous Fe-bearing industrial wastes and can be regarded as a first step of a standardization procedure, necessary for future process scaling and design.

## CRediT authorship contribution statement

**Ismael Fuentes:** Methodology, Validation, Investigation. **Claudia Ulloa:** Conceptualization. **Romel Jiménez:** Methodology, Formal analysis, Visualization, Data curation. **Ximena García:** Conceptualization, Investigation, Formal analysis, Supervision, Funding acquisition.

## Declaration of Competing Interest

The authors declare that they have no known competing financial interests or personal relationships that could have appeared to influence the work reported in this paper.

## Acknowledgments

The authors acknowledge the financial support of CONICYT-Chile through the Fondecyt Project 1140410. Support of the University of Concepción is also strongly recognized (VRID Project 213.096.064-10 and a scholarship to I. Fuentes).

## References

Alzeer, M., MacKenzie, K., 2018. Synthesis and catalytic properties of new sustainable aluminosilicate heterogeneous catalysts derived from fly ash. ACS Sustain. Chem. Eng. 6 (4), 5273–5282. https://doi.org/10.1021/acssuschemeng.7b04923.

Bartholomew, C., Farrauto, R., 1976. Chemistry of nickel-alumina catalyst. J. Catal. 45, 41–53. https://doi.org/10.1016/0021-9517(76)90054-3.

Cano, L.A., García Blanco, A.A., Lener, G., Marchetti, S.G., Sapag, K., 2017. Effect of the support and promoters in Fischer-Tropsch synthesis using supported Fe catalyst. Catal. Today 282, 204–213. https://doi.org/10.1016/j.cattod.2016.06.054.

Cardona, N., Coursol, P., Vargas, J., Parra, R., 2013. The physical chemistry of copper smelting slags and copper losses at the paipote SmelterPart 2 –characterisation of industrial slags. Can. Metall. Q. 50, 330–340. https://doi.org/10.1179/000844311X13112418194806.

Cheng, J., Zhou, F., Xuan, X., Liu, J., Zhou, J., Cen, K., 2017. Comparison of the catalytic

effects of eight industrial wastes rich in Na, Fe, Ca and Al on anthracite coal combustion. Fuel 187, 398–402. https://doi.org/10.1016/j.fuel.2016.09.083.
de la Caba, K., Guerrero, P., Si, T., Cruz-Romero, M., Kerry, J., Fluhr, J., Maurer, M., Kruijssen, F., Albalat, A., Bunting, S., Burt, S., Little, D., Newton, R., 2019. From seafood waste to active seafood packaging: an emerging opportunity of the circular economy. J. Clean. Prod. 208, 86–98. https://doi.org/10.1016/j.jclepro.2018.09.164.
Deng, Z., Huang, Z., He, F., Zheng, A., Wei, G., Meng, J., Zhao, Z., Li, H., 2019. Evaluation of calcined copper slag as an oxygen carrier for chemical looping gasification of sewage sludge. Int. J. Hydrogen Energy 44, 17823–17834. https://doi.org/10.1016/j.ijhydene.2019.05.039.
Derouane, E., Simoens, A., Colin, C., Martin, G., Dalmon, J., Védrine, J., 1978. Effects of particle size and degree of reduction on the magnetic properties of dispersed nickel catalysts. J. Catal. 52, 50–58. https://doi.org/10.1016/0021-9517(78)90122-7.
Dhir, R., Brito, J., Mangabhai, R., Qun, C., 2017. Sustainable Construction Materials: Copper Slag, 1st edition. Woodhead Publishing, an imprint of Elsevier, Duxford, U.K. https://doi.org/10.1016/C2015-0-00465-8.
Dilmac, N., Yörük, S., Gülaboglu, S., 2012. Determination of reduction degree of direct reduced iron via FT-IR spectroscopy. Vib. Spectrosc. 61, 25–29. https://doi.org/10.1016/j.vibspec.2012.03.008.
Gao, J., Liu, Q., Gu, F., Liu, B., Zhong, Z., Su, F., 2015. Recent advances in methanation catalyst for the production of synthetic natural gas. RSC Adv. 5, 22759–22776. https://doi.org/10.1039/c4ra16114a.
Gorai, B., Jana, R., 2003. Characteristics and utilization of copper slag. Resour. Conserv. Recycl. 39, 299–313. https://doi.org/10.1016/S0921-3449(02)00171-4.
Govender, N., Gideon, F., Croon, M., Schouten, J., 2008. Mechanistic pathway for methane formation over an iron-based catalyst. J. Catal. 260, 254–261. https://doi.org/10.1016/j.jcat.2008.10.008.
Guo, Z., Pan, J., Zhu, D., Zhang, F., 2018a. Green and efficient utilization of waste ferric-oxide desulfurizer to clean waste copper slag by the smelting reduction-sulfurizing process. J. Clean. Prod. 199, 891–899. https://doi.org/10.1016/j.jclepro.2018.07.203.
Guo, Z., Zhu, D., Pan, J., Zhang, F., 2018b. Innovative methodology for comprehensive and harmless utilization of waste copper slag via selective reduction-magnetic separation process. J. Clean. Prod. 187, 910–922. https://doi.org/10.1016/j.jclepro.2018.03.264.
Huanosta, T., Danta, R., Ramírez, R., Esplugas, S., 2012. Evaluation of copper slag to catalyze advanced oxidation processes for the removal of phenol in water. J. Hazard. Mater. 213–214, 325–330. https://doi.org/10.1016/j.jhazmat.2012.02.004.
Jin, G., Gu, F., Liu, Q., Wang, X., Jia, L., Xu, G., Zhong, Z., Su, F., 2016. Highly stable Ni/SiC catalyst modified by $Al_2O_3$ for CO methanation reaction. RSC Adv. 6, 9631–9639. https://doi.org/10.1039/c5ra19940a.
Jurgilevich, A., Birge, T., Kentala-Lehtonen, J., Korhonen-Kurki, K., Pietikäinen, J., Saikku, L., Schösler, H., 2016. Transition towards circular economy in the food system. Sustainability 8https://doi.org/10.3390/su8010069. 69-x.
Langford, J., Wilson, A., 1978. Scherrer after sixty years: a survey and some new results in the determination of crystallite size. J. App. Crystallogr. 11, 102–113. https://doi.org/10.1107/S0021889878012844.
Lee, G., Song, J., Lee, J., 2016. Reaction kinetics and phase transformation during hydrogen reduction of spherical $Fe_2O_3$ nanopowder agglomerates. Powder Technol. 302, 215–221. https://doi.org/10.1016/j.powtec.2016.07.038.
Li, J., Cheng, X., Zhang, C., Chang, Q., Wang, J., Wang, X., Lv, Z., Dong, W., Yang, Y., Li, Y., 2016. Effect of alkalis on iron-based Fischer Tropsch synthesis catalyst: alkali-FeOx interation, reduction and catalytic performance. Appl. Catal. A Gen. 528, 131–141. https://doi.org/10.1016/j.apcata.2016.10.006.
Li, H., Li, H., Deng, J., 2000. Influence on the reduction degree of Ni–B/SiO2 amorphous catalyst and its role in selective hydrogenation of acrylonitrile. Appl. Catal. A 193, 9–15. https://doi.org/10.1016/S0926-860X(99)00422-6.
Lori, A., Hassani, A., Sedghi, R., 2019. Investigating the mechanical and hydraulic characteristics of pervious concrete containing copper slag as coarse aggregate. Constr. Build. Mater. 197, 130–142. https://doi.org/10.1016/j.conbuildmat.2018.11.230.
Luo, M., Hamdeh, H., Davis, B.H., 2009. Fischer Tropsch Synthesis Catalyst activation of low alpha iron catalyst. Catal. Today 140, 127–134. https://doi.org/10.1016/j.cattod.2008.10.004.
Madon, R., Boudart, M., 1982. Experimental criterion for the absence of artifacts in the measurement of rates of heterogeneous catalytic reactions. Ind. Eng. Chem. Fundam. 21, 438–447. https://doi.org/10.1021/i100008a022.
Marwaha, A., Rosha, P., Kumar Mohapatra, S., Kumar Mahla, S., Dhir, A., 2018. Waste materials as potential catalyst for biodiesel production: current state and future scope. Fuel Process Technol. 181, 175–186. https://doi.org/10.1016/j.fuproc.2018.09.011.
Mills, G., Steffgen, F., 1973. Catalytic methanation. Catal. Rev. 8, 159–210. https://doi.org/10.1080/01614947408071860.
Nakhaei, A., Reza, M., Faramarz, S., Zarkesh, J., 2010. Deactivation studies of Fischer-Tropsch synthesis on nano-structured iron catalyst. J. Mol. Catal. A Chem. 330, 112–120. https://doi.org/10.1016/S1003-9953(09)60061-X.
Niemantsverdriet, J., Van Der Kraan, A., 1981. On the time-dependent behavior of iron catalyst in Fischer-Tropsch Synthesis. J. Catal. 72, 385–388. https://doi.org/10.1016/0021-9517(81)90025-7.
Norrish, K., Taylor, R., 1962. Quantitative Analysis By X-Ray Diffraction, Division of Soils, Adelaide. http://docplayer.net/25884649-Quantitative-analysis-by-x-ray-diffraction.html.
Ocampo, F., Louis, B., Kiwi-Minsker, L., Roger, A.C., 2011. Effect of Ce/Zr composition and noble metal promotion on nickel based $Ce_xZr_{1-x}$ catalyst for carbon dioxide methanation. Appl. Catal. A 392, 36–44. https://doi.org/10.1016/j.apcata.2010.10.025.
Oh, J., Noh, D., 2017. The reduction kinetics of hematite particles in H2 and CO atmospheres. Fuel 196, 144–153. https://doi.org/10.1016/j.fuel.2016.10.125.
Piotrowski, K., Mondal, K., Lorethova, H., Stonawski, L., Szymanski, T., Wiltowski, T., 2005. Effect of gas composition on the kinetics of iron oxide reduction in a hydrogen production process. Int. J. Hydrogen Energy 30, 1543–1554. https://doi.org/10.1016/j.ijhydene.2004.10.013.
Potysz, A., Kierczak, J., Pietranik, A., Kadziolka, K., 2018. Mineralogical, geochemical, and leaching study of historical Cu-slags issued from processing of the Zechstein formation (Old Copper Basin, southwestern Poland). Appl. Geochem. 98, 22–35. https://doi.org/10.1016/j.apgeochem.2018.08.027.
Raposeiras, A., Movilla, D., Bilbao, R., Cifuentes, C., Ferrer, G., Castro, D., 2018. The use of copper slags as an aggregate replacement in asphalt mixes with RAP: physical-chemical and mechanical behavioural analysis. Constr. Build. Mater. 190, 427–438. https://doi.org/10.1016/j.conbuildmat.2018.09.120.
Riedel, T., Schulz, H., Scahub, G., Jun, K.W., Soo Hwang, J.S., Lee, K.W., 2003. Fischer Tropsch on iron $H_2/CO$ and $H_2/CO_2$ as synthesis gases. The episodes of formation of the Fischer Tropsch regime and construction of the catalyst. Top. Catal. 26, 41–544. https://doi.org/10.1023/B:TOCA.0000012986.46680.28.
Rojas, S., Fierro, J., Herranz, T., Pérez, F., Ojeda, M., Terreros, P., 2006. Genesis of iron carbides and their role in the synthesis of hydrocarbons from synthesis gas. J. Catal. 243, 199–211. https://doi.org/10.1016/j.jcat.2006.07.012.
Rönsch, S., Schneider, J., Matthischke, S., Schlüter, M., Götz, M., Lefevre, J., Prabhakaran, P., Bajohr, S., 2016. Review on methanation- from fundamentals to current projects. Fuel 166, 276–296. https://doi.org/10.1016/j.fuel.2015.10.111.
Sarfo, P., Das, A., Wyss, G., Young, C., 2017. Recovery of metal values from copper slag and reuse of secondary slag. Waste Manage. 70, 272–281. https://doi.org/10.1016/j.wasman.2017.09.024.
Sharma, R., Khan, R., 2018. Influence of copper slag and metakaolin on the durability of self compacting concrete. J. Clean. Prod. 171, 1171–1186. https://doi.org/10.1016/j.jclepro.2017.10.029.
Shih, K., Li, H., Zhang, W., Wang, J., Yang, Z., Li, L., 2018. Copper slag as catalyst for mercury oxidation in coal combustion flue gas. Waste Manage. 74, 253–259. https://doi.org/10.1016/j.wasman.2017.11.044.
Shroff, M., Kalakkad, D., Coulter, K., Köhler, S., Harrington, M., Jackson, N., Sault, A., Datye, A., 1995. Activation of precipitated iron Fischer Tropsch synthesis catalyst. J. Catal. 156, 185–207. https://doi.org/10.1006/jcat.1995.1247.
Vannice, M., 1975. The catalytic synthesis of hydrocarbons from $H_2/CO$ mixtures over the group VIII metals: I. J. Catal. 37 (1975), 449–461. https://doi.org/10.1016/0021-9517(75)90181-5.
Vannice, M., 1977. The catalytic synthesis of hydrocarbons from $H_2/CO$ mixtures over the group VIII metals: V. J. Catal. 50, 228–236. https://doi.org/10.1016/0021-9517(77)90031-8.
Wan, H., Wu, B., Tao, Z., Li, T., An, X., Xian, H., Li, Y., 2006. Study of an iron-based Fischer-Tropsch synthesis catalyst incorporated with $SiO_2$. J. Mol. Catal. A Chem. 260, 255–263. https://doi.org/10.1016/j.molcata.2006.07.062.
Wang, X., Fu, G., Li, W., Zhu, M., 2019. Numerical simulation of effect of operating conditions on flash reduction behaviour of magnetite under H2 atmosphere. Int. J. Hydrogen Energy 44, 26261–26270. https://doi.org/10.1016/j.ijhydene.2019.08.089.
Yu, W., Sun, Y., Lei, M., Chen, S., Qiu, T., Tang, Q., 2019. Preparation of micro-electrolysis material from flotation waste of copper slag and its application for degradation of organic contaminants in water. J. Hazard. Mater. 361, 221–227. https://doi.org/10.1016/j.jhazmat.2018.08.098.
Ziegler, T., Lo, J., 2007. Density functional theory and kinetic studies of methanation on iron surface. J. Phys. Chem. 111, 11012–11025. https://doi.org/10.1021/jp0722206.